

## Electronic structure and tunneling resonance spectra of nanoscopic aluminum islands

Gustavo A. Narvaez and George Kirczenow

Department of Physics, Simon Fraser University, Burnaby, British Columbia, Canada, V5A 1S6  
(November 9, 2021)

The electronic structure of nanoscopic oxide-coated aluminum islands is investigated using a tight-binding model that incorporates the geometry, chemistry and disorder of the particle. The oxide coat is found to significantly increase the volume accessible to electrons at the Fermi level. The level statistics agree with random matrix theory predictions. States near the Fermi level show pronounced clustering regardless of disorder. It is suggested that the observed clusters of tunneling resonances may have a more complex origin than if they were solely due to many-body non-equilibrium effects.

PACS numbers: 73.22.-f, 73.22.Dj

It is expected that the statistics of the discrete energy spectra of small disordered metal grains should be described by random matrix theory (RMT) [1]. Experimental confirmation of RMT predictions for such systems, however, presents a challenge. Recently, some of the technological difficulties have been overcome and electron tunneling spectroscopy experiments have been carried out on Al, Au and Co nanoscopic particles [2-4]. These transport experiments have opened the possibility of testing directly the applicability of RMT to the energy spectra of these nanoscopic metal islands (nanoislands).

The observed electron tunneling spectra of Al nanoislands coated with aluminum oxide [2] showed a surprisingly high density and pronounced clustering of conductance resonances. A gam and co-workers [5] proposed that this unexpected behavior is a manifestation of the effects of electron-electron interactions on non-equilibrium states of the nanoislands. By focusing on the many-body aspects of the problem, they were able to account for the anomalous features of the data qualitatively in an appealing way. However, they modeled the underlying one-electron spectra of the nanoislands phenomenologically. For a complete understanding of the experiments a microscopic treatment of the single-electron energy spectra is desirable. Microscopic models of aluminum nanostructures have been proposed [6], but none of those works addressed the electronic structure or transport properties of Al nanoislands similar to those in the above experiments. Recently, Campbell et al. performed state-of-the-art molecular dynamics simulations of the passivation of Al nanospheres with aluminum oxide but did not calculate the electronic spectra of the particles [7].

In this communication, we present microscopic tight-binding calculations of the single-electron electronic spectra of Al nanoislands coated with Al-oxide. We include the geometry, atomic lattice, chemistry and disorder of the nanoparticle explicitly in our theory. Our leitmotiv is twofold: i) comparison of RMT predictions for the energy spectra of generic disordered metal grains with the electronic structure obtained from realistic numerical simulations; and ii) improvement of our understanding of the experimentally observed tunneling resonance spectra.

Motivated by the experiment, we consider a hemispherical nanoparticle of volume  $V = 40\text{nm}^3$ , and investigate the effects of the disorder at the metal/oxide interface on the electronic structure and transport properties. (Different geometries yield qualitatively similar results.) We start with an analysis of the mean level spacing and level fluctuations in the neighborhood of the Fermi energy of the particles. We find that describing the discrete energy levels in this region according to RMT should be a satisfactory starting point when dealing with Al nanoislands coated with Al-oxide. However, the magnitude of the calculated mean level spacing is consistent with a significant enhancement of the effective electronic volume of metallic nanoparticle due to the presence of the oxide coat. Next, a closer look at a few levels around the Fermi level reveals a rich electronic structure: There are clusters of levels and the clustering is strongly affected by the specifics of disorder. Furthermore, the clustering of the single-electron energy levels persists even in the presence of severe interface disorder. Finally, we model the differential conductance ( $dI=dV$ ) spectrum and find clusters of tunneling resonances. The clustering is due to the complex structure of energy levels around the Fermi energy of the particle. The clusters of resonances are sensitive to disorder and to the capacitances of the tunnel junctions. The predicted number of tunneling resonances is not sufficient to explain the experimental data [2] within a purely single-electron picture of transport. Nonetheless, our results suggest that the observed clusters of tunneling resonances [2] may have a more complex origin than if they were solely due to many-body non-equilibrium effects during transport.

We assume that the Al atoms in the interior of the nanoparticle form an fcc lattice with a lattice parameter  $a = 0.405\text{nm}$ . The atoms at the surface of the nanoparticle have a different coordination number from the bulk fcc lattice. This establishes a criterion for defining the surface of the particle. In addition, the Al nanoislands in the experiment were passivated with a thin Al-oxide layer which acts as a tunnel barrier between the particle and leads. This layer also imposes some structural disorder at the metal-oxide interface. We model this metal-oxide in-

interface in the following way: First, we define which atoms of the particle belong to the surface and identify this region as the interface; second, we randomly choose some of those sites (approximately 50%) to represent O atoms while the others correspond to Al. In the first part of this procedure we adopt two different criteria: Criterion 1 ( $C_1$ ): We assume the surface atoms to be those whose first neighbor coordination number is not equal to that of an fcc lattice. Criterion 2 ( $C_2$ ): Surface atoms are those whose first and/or second neighbor coordination numbers are not equal to those of an fcc lattice. The random choice of O and Al atoms in the metal-oxide interface is the only source of disorder in the results presented here.

We use a multiband (s, p, and d valence orbitals) tight-binding Hamiltonian without spin-orbit coupling:

$$H = \sum_i \sum_{\alpha} X_{i\alpha} c_{i\alpha}^\dagger c_{i\alpha} + \sum_{ij} \sum_{\alpha\beta} X_{ij\alpha\beta} c_{i\alpha}^\dagger c_{j\beta} + \text{h.c.} \quad (1)$$

$i, j$  label the atoms,  $c_{i\alpha}^\dagger$  ( $c_{i\alpha}$ ) creates (destroys) an electron on site  $i$ , and the index  $\alpha$  indicates the s, p or d orbital.  $X_{i\alpha}$  and  $X_{ij\alpha\beta}$  are the Slater-Koster (SK) [8] on-site and hopping (up to second neighbors) parameters. We adopt an SK model in which the atomic orbitals on different sites are orthonormal. For the Al sites in the interior (bulk) of the particle we used the SK parameters given in Ref. [9]. The Al and O sites in the metal-oxide interface have different SK parameters as is discussed below. The bonding of the atoms that form the oxide layer is due to charge transfer from the Al to the O. Campbell et al. have shown that the metal-oxide interface of spherical Al nanoparticles consists mainly of intercalated  $O^{1=2}$  and  $Al^{1=2}$  [7]. These valence charges determine the SK on-site parameters for the interface atoms which we calculate following the Mulliken-Wolfsberg-Helmholz molecular-orbital approach [10]. We determine the nearest neighbor O-Al hopping parameters by assuming an average separation of 0.18 nm [7] between O and Al atoms in the oxide, applying Harrison's model to obtain the two-center transfer integrals [11] and then transforming them to find the SK hopping parameters [9]. The same procedure is applied to find the nearest neighbor O-O hopping, using 0.30 nm [12] as the average separation between O atoms. The SK hopping parameters between Al atoms are assumed to be the same regardless of the valence charge.

We now present our results for a nanoisland of volume  $V = 40.45 \text{ nm}^3$  for different realizations of disorder and surface criteria  $C_1$  and  $C_2$ . For this volume the particle-in-a-box (SP) mean level spacing  $\Lambda_{SP}^1 = (4E_F^{\text{Al}} - 3N)/V = 2.09 \text{ meV}$  where  $E_F^{\text{Al}}$  is the Fermi energy and  $N$  the electron density of bulk Al. The total number of atoms is  $N = 2587$  and the surface-to-bulk ratio is  $(N_S/N_B)_1 = 0.538$  and  $(N_S/N_B)_2 = 0.970$  for criteria  $C_1$  and  $C_2$ , respectively. Note that for  $C_1$  the nanoisland is primarily bulk while for  $C_2$  it is almost evenly balanced between bulk and surface. In the latter case the disorder is particularly severe. In Table I we

present, for both  $C_1$  and  $C_2$ , the number of  $O^{1=2}$  ( $N_O$ ) and  $Al^{1=2}$  ( $N_{Al}$ ) atoms, the total number of electrons ( $n$ ) in the nanoisland, the calculated Fermi energy ( $E_F$ ), and the calculated mean energy level separation  $\Delta$ .  $E_F$  is the energy of the highest occupied level assuming that spin up and down levels are degenerate. We find that the value of  $E_F$  does not show major changes when switching from  $C_1$  to  $C_2$ . It seems that the increase in  $n$ , due to the increased metal-oxide interface, in going from  $C_1$  to  $C_2$  is compensated by the associated changes in the electronic structure of the particles. This compensation keeps  $E_F$  almost independent of the surface criteria. Surprisingly, we see that the different choices of surface criteria have a minimal effect on the values of  $\Delta$ . Additionally, these values of  $\Delta$  agree well with  $\Lambda_{SP}^1$ . These two findings are non-trivial and important: They imply that the mean level separation around  $E_F$  is determined not by the volume of the aluminum core of the nanoparticle but by a larger volume that includes part of the oxide coat. For small particles with large surface to volume ratios this should have a significant effect (exceeding a factor of 2) on the mean level spacing which should be reflected in the experimental spectra. However, a qualitatively similar enhancement of the value of the nanoisland volume that is deduced from the experimental capacitance measurements of the tunnel junctions [2] may also be possible. In this work the total volume  $V$  that determines  $\Lambda_{SP}^1$  is kept fixed at an experimentally estimated value for the different disorder realizations and surface criteria.

We now discuss the statistics of the energy levels that we find around  $E_F$ . In each spectrum, we select a symmetric energy interval (of 400 meV) around  $E_F$  containing  $p = 200$  levels. Then we find the nearest level energy spacing  $E_t = \epsilon_{t+1} - \epsilon_t$  for each level  $t$  in the chosen set, and the mean level spacing  $\Delta = (1/p) \sum_{t=1}^p E_t$ . To compare our results with the RMT prediction, we build a histogram of the calculated spacings using a bin size  $\Delta = \Delta/5$ . Figure 1(a) shows such histograms for representative realizations of criteria  $C_1$  and  $C_2$ . The energy is in normalized units:  $s = E_t/\Delta$ . In RMT our system falls into the orthogonal ensemble due to its time reversal symmetry. In this case, the Wigner distribution  $P_W(s) = (\pi/2) \exp(-\pi s^2/4)$  is a good approximation to the distribution predicted for the Gaussian orthogonal ensemble (GOE) for the probability of finding a spacing  $E_t = \Delta s$  in the interval  $(s; s + ds)$  [1]. We see from Fig. 1(a) that the probability of finding a spacing  $E_t = \Delta s$  in the interval  $(s; s + \Delta]$  (histogram) is well described by  $P_W(s) \Delta$  (thin-solid line) irrespective of the surface criteria.

In general, given a set of  $q$  levels, neighboring level distributions  $P_k(s)$  are defined as the probability of finding a spacing  $E_t^k$  containing  $k$  adjacent levels in the interval  $(s; s + ds)$ . The case  $k = 0$  corresponds to the nearest level spacing distribution discussed above. The statistical properties of  $P_k(s)$  are well established for the GOE [1]. In particular, specific results hold for the standard deviation (or width)  $\Delta_k$  of these distributions [13]. We now compare our numerical findings with the GOE pre-

distributions. Formally,  $(\epsilon_k)^2 = \langle \epsilon_k^2 \rangle = \frac{1}{N} \sum_{t=1}^N (E_t^k - \bar{E}_k)^2$  for the  $k$ -spacing:  $E_t^k = E_{k+t+1} - E_t$  between levels  $k+t+1$  and  $k$ ,  $\bar{E}_k$  the mean of  $E_t^k$ , and  $\epsilon_k = E_k - E_0$ . Note that according to this definition  $\epsilon_k$  is expressed in units of  $E_F$ . Figure 1(b) shows the GOE prediction (solid line) for  $\epsilon_k$  and the values (symbols) found with the above set of calculated energy levels for different disorder realizations. For both surface criteria, the calculated values of  $\epsilon_k$  scatter around the GOE prediction. For criterion  $C_2$ , where surface is a large fraction of the particle, the scatter is stronger. Although the number of disorder realizations shown is too small for accurate ensemble averaging, the calculated  $\epsilon_k$  are consistent with the RMT trend.

We now consider the details of the electronic structure in a smaller region around  $E_F$ . Figure 2 is a plot of the first few levels around  $E_F$  for five disorder realizations for each surface criterion. The energy is measured relative to  $E_F$  in units of  $\frac{A_1}{S_P}$ . The levels present a rich structure and are far from being equally-spaced by the energy  $\frac{A_1}{S_P}$ . We find that most of the levels form groups of two or more. The results are qualitatively similar for  $C_1$  and  $C_2$ , however, the details around  $E_F$  are set by disorder and surface criteria. Note that the predicted number of levels ( $\approx 19$ ) for all disorder realizations (with exception to #1 and #6) studied here is fairly consistent with the number of levels expected from the SP model in the considered energy range:  $[10; 10] \frac{A_1}{S_P}$ . It is important to note that the clustering seen in the spectra is taking place in the presence of disorder in the metal-oxide interface. Although we have shown that in a wider range of energy around  $E_F$  the probability of finding strong bunching of levels is small, this does not mean that pairs or larger clusters are avoided in a small neighborhood around  $E_F$ .

We now turn to the implications of this clustering of energy levels for experimental tunnel resonance spectra of the nanoislands. The orthodox model of the device (nanoisland + tunnel junctions + leads) treats the leads as reservoirs of electrons with chemical potentials  $\mu_L$  and  $\mu_R$ , coupled capacitively (with capacitances  $C_L$  and  $C_R$ ) to the nanoisland through the tunneling junctions. The applied voltage  $V$  between the leads is divided between  $C_L$  and  $C_R$  setting the electrochemical potential in the right (left) lead to  $\mu^+ (\mu^-) = \mu_R (L) + (e) (C_L (C_R) = C) eV$  with  $C = C_L + C_R$ . When  $V = 0$ ,  $\mu_L$  and  $\mu_R$  are considered aligned with  $E_F$ . As discussed by Averin and Korotkov [14], the discrete energy spectrum of the nanoisland allows tunneling to occur whenever  $\mu^+ (\mu^-)$  (measured from  $E_F$ ) matches the energy of one of the available levels of the nanoisland. Figure 3 shows the predicted [15]  $dI=dV$  spectra for different disorder realizations and surface criteria. The resonances are marked with at-top (bottom) segments indicating that  $\mu^+ (\mu^-)$  has originated the resonance. Two different regimes: i) (Fig. 3(a)) symmetric ( $C_L = C_R$ ), and ii) (Fig. 3(b)) non-symmetric ( $C_L = 1.5aF$  and  $C_R = 3.2aF$  [2]) tunneling junctions were considered. The  $dI=dV$  spectra arising from a model with equally spaced energy levels is shown (solid circles) for comparison. Clearly, the clustering in

the energy spectra creeps into the  $dI=dV$  spectra in a non-trivial way. The nature of the clusters of resonances in the  $dI=dV$  spectrum is strongly dependent on disorder and on the relative values of  $C_L$  and  $C_R$ .

Now we show that the clustering of resonances present in the calculated  $dI=dV$  qualitatively resembles the observed clustering. Experimentally (Fig. 1(a) of Ref. [5]), the clusters of resonances observed are as follows: i) a single resonance at the beginning of the spectrum (this sets the origin of energies), ii) 4 near-by resonances around  $\frac{A_1}{S_P}$ , iii) 2 near-by resonances located at  $1.5 \frac{A_1}{S_P}$ , and iv) 4 resonances distributed over an energy interval equal to  $\frac{A_1}{S_P}$  centered around  $2.5 \frac{A_1}{S_P}$ . We choose spectrum #4 in the symmetric and non-symmetric regime, under criterion  $C_1$ , for comparison with the experiment. In the symmetric regime the spectrum shows: i) a single resonance at the origin, ii) 2 pairs of resonances located around  $\frac{A_1}{S_P}$  and  $2 \frac{A_1}{S_P}$ , respectively, and iii) 4 near-by resonances spanning an energy interval approximately equal to  $\frac{A_1}{S_P}$ , around  $3.5 \frac{A_1}{S_P}$ . When switching to the non-symmetric regime (the experimental regime) the structure of the clustering is slightly modified, with the overall number of resonances smaller. We see, then, that the observed and calculated clusters show qualitative common features. Whether the energy scales ( $\frac{A_1}{S_P}$ ) on which the theoretical and experimental clusterings occur are similar or not remains an open question: This depends on what the correct value of the effective volume of the Al island is. We have shown that this volume may be significantly larger than has been assumed previously. If this is the case then the experimental and theoretical energy scales may be very similar; letting the experiment be explained in a new way.

Finally, if we further assume that non-equilibrium many-body effects such as those described by Agam et al. [5] are present then still more clustering appears in the spectrum as most of the single-electron transport resonances in Fig. 3 split to become clusters of resonances. However, our results indicate that the observed tunneling resonance spectra should show a different behavior from what would follow from the simple equidistant-level model of the underlying single-electron spectrum that has been assumed in previous analyses of the experiments, whether many-body non-equilibrium effects are present or not.

Support from NSERC and CIAR is acknowledged.

- 
- [1] M. L. M ehta, Random Matrices (Academic Press, New York, 1991); W. P. Halperin, Rev. Mod. Phys. 58, 533 (1986); K. B. Efetov, Adv. Phys. 32, 53 (1983); T. A. Brody et al., Rev. Mod. Phys. 53, 385 (1981)
  - [2] D. C. Ralph, C. T. Black, and M. Tinkham, Phys. Rev. Lett. 74, 3241 (1995); Physica 218B, 258 (1996)
  - [3] D. D avidovic, M. Tinkham, Phys. Rev. Lett. 83, 1644 (1999)

- [4] S. Gueron et al., Phys. Rev. Lett. 83, 4148 (1999)  
[5] O. A. Gam, N. S. W. ingreen, B. L. A. Itshuler, D. C. Ralph, and M. Tinkham, Phys. Rev. Lett. 78, 1956 (1997)  
[6] F. Cyrot-Lackmann et al., J. Phys. (Paris) 38, C2-57 (1977); T. N. Todorov et al., J. Phys. Condes. Matter 5, 2389 (1993); N. D. Lang, Phys. Rev. B 52, 5335 (1995); G. Taraschi, J. L. Mozos, C. C. Wan, H. Guo, and J. Wang, Phys. Rev. B 58, 13 138 (1998)  
[7] T. Campbell, R. K. Kalia, A. Nakano, P. Vashishta, S. Ogata, S. Rodgers, Phys. Rev. Lett. 82, 4866 (1999)  
[8] J. C. Slater and G. F. Koster, Phys. Rev. 94, 1498 (1954)  
[9] D. A. Papaconstantopoulos, Handbook of the Band Structure of Elemental Solids (Plenum, New York, 1986)  
[10] S. P. McGlynn, et al., Introduction to Applied Quantum Chemistry (Holt, Rinehart, Winston, New York, 1972).  
[11] W. A. Harrison, Electronic Structure and the Properties of Solids (Freeman, San Francisco, 1980)  
[12] S. Ansell et al., Phys. Rev. Lett. 78, 464 (1997)  
[13] O. Bohigas, M. J. G. iannoni, Ann. Phys. (NY) 89, 393 (1975)  
[14] D. V. Averin and A. N. Korotkov, Zh. Eksp. Teor. Fiz. 90, 1056 (1986) [Sov. Phys. JETP 70, 937 (1990)]  
[15] Here we omit the Coulomb blockade energy  $E_C$  of adding one electron to the nanoisland. Including this would cause an upwards rigid shift of the resonances by an amount  $E_C$ . Experimentally, this energy is  $\sim 0.5$  meV.

C <sub>1</sub>						C <sub>2</sub>					
label	N <sub>O</sub>	N <sub>AL</sub>	n	E <sub>F</sub> (eV)	(meV)	label	N <sub>O</sub>	N <sub>AL</sub>	n	E <sub>F</sub> (eV)	(meV)
# 1	444	461	9093	8.297	2.34	# 6	651	623	9714	8.483	2.32
# 2	448	457	9105	8.313	2.30	# 7	634	640	9663	8.370	2.30
# 3	451	454	9114	8.330	2.30	# 8	632	642	9657	8.383	2.32
# 4	440	465	9081	8.293	2.31	# 9	630	644	9651	8.348	2.34
# 5	434	471	9063	8.251	2.32	# 10	629	645	9648	8.336	2.35

TABLE I. Parameters characterizing the nanoparticles. C<sub>1</sub> and C<sub>2</sub> are criteria that determine the surface (see text).

FIG. 1. (a) Probability distribution (histograms) for the nearest level spacings and Wigner distribution (thin solid line). (b) Standard deviation  $\sigma_k$  for different disorder realizations (points) and the GOE prediction (solid line). C<sub>1</sub> and C<sub>2</sub> as in Table 1.

FIG. 2. Energy levels for different disorder realizations (see text). C<sub>1</sub> and C<sub>2</sub> as in Table 1.

FIG. 3. dI=dV spectra for different disorder realizations and capacitance regimes (see text). C<sub>1</sub> and C<sub>2</sub> as in Table 1.

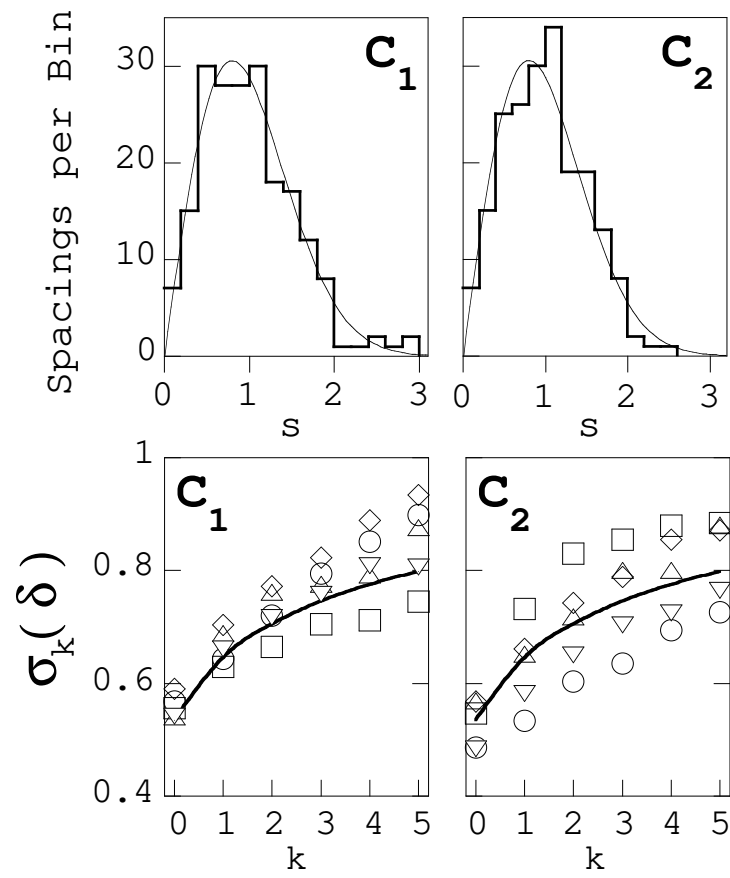


Figure 1, Narvaez and Kirczenow

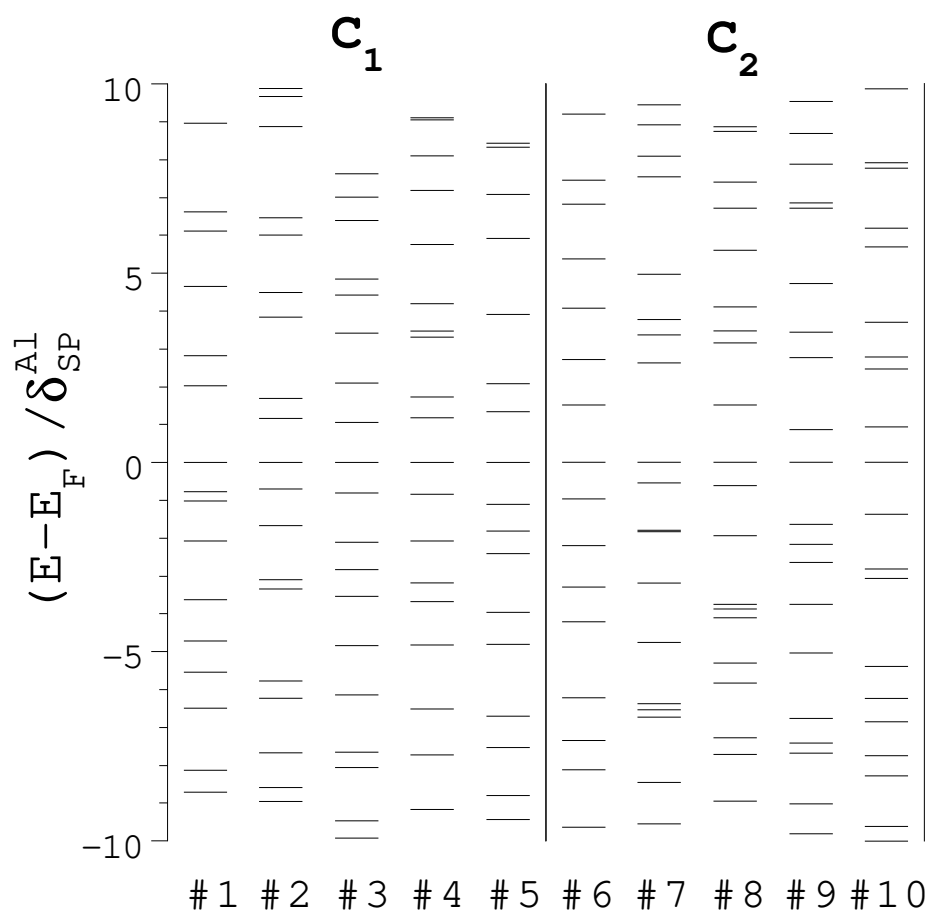


Figure 2, Narvaez and Kirczenow

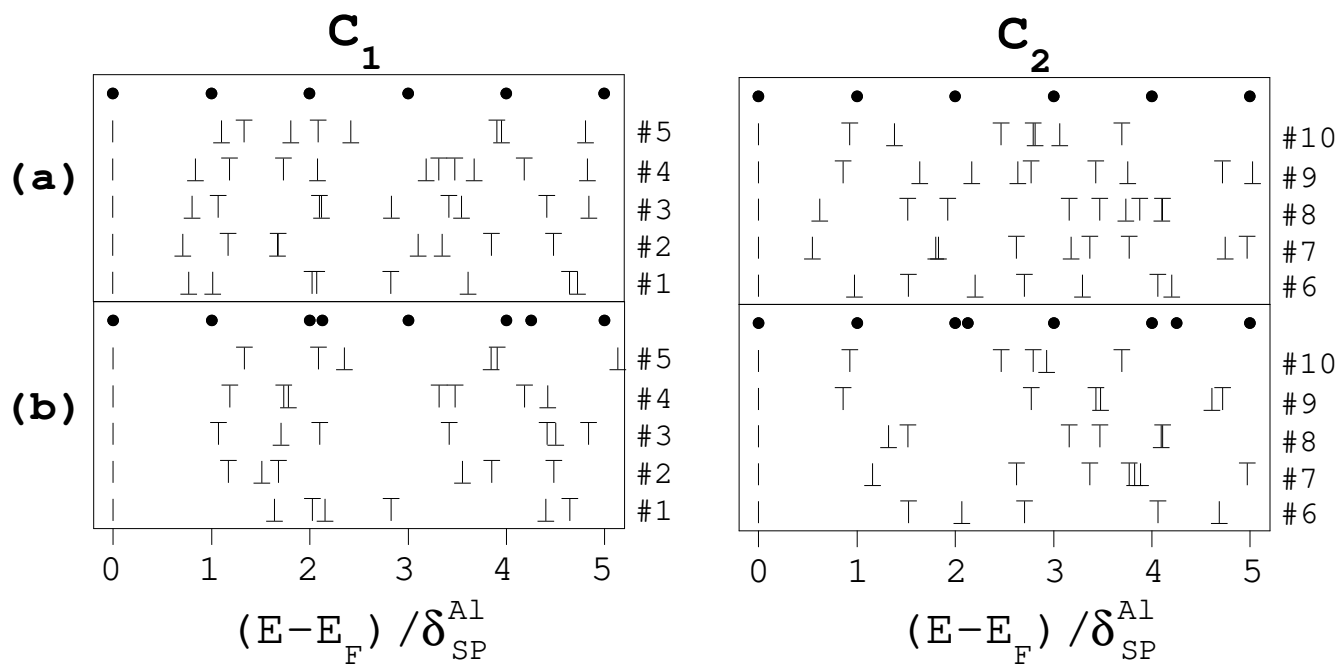


Figure 3, Narvaez and Kirczenow